VIII International Conference on Fracture Mechanics of Concrete and Concrete Structures
FraMCoS-8
J.G.M. Van Mier, G. Ruiz, C. Andrade, R.C. Yu and X.X. Zhang (Eds)

XFEM USING A NON LINEAR FRACTURE MECHANICS APPROACH FOR CONCRETE CRACK PROPAGATION IN DAM SAFETY ASSESSMENT

Simon-Nicolas Roth*, Pierre Léger† and Azzeddine Soulaïmani††

*Hydro-Québec
75 boul. René-Lévesque Ouest, Montréal, Québec, Canada, H2Z 1A4
e-mail: roth.simon-nicolas@hydro.qc.ca, www.hydroquebec.com

†École Polytechnique de Montréal
Department of Civil, Geological and Mining Engineering
C.P. 6079, succ. Centre-Ville, Montréal Québec, Canada, H3C 3A7
e-mail: pierre.leger@polymtl.ca, www.polymtl.ca

††École de Technologie Supérieure
Department of Mechanical Engineering
1100, rue Notre-Dame Ouest, Montréal, Québec, Canada, H3C 1K3
e-mail: azzeddine.soulaimani@etsmtl.ca, www.etsmtl.ca

Key words: Crack Tracking Technique, Non Linear Fracture Mechanics, Extended Finite Element Method, Continuum Damage Model

Abstract. This paper presents a crack model that couples the benefits of the damage mechanics approach and the extended finite element method (XFEM). A local crack-tracking technique is developed to propagate a crack pattern along a single row of finite elements as a function of the equivalent principal stress direction. The level-sets are computed to predict the crack path and with the use of continuum damage mechanics, the path is corrected. Once a certain level of damage is reached inside an element, the level-sets computed previously are used to apply the XFEM formulation with Heaviside function within this element introducing a discontinuity in the displacement field. The three point beam tested by Bažant and Pfeiffer, the shear beam with single notch tested by Arrea and Ingraffea and the tension-shear specimen tested by Nooru-Mohamed are used for the validation of the proposed model that is targeted to be used shortly in dam safety application.

1 Introduction

The effect of cracks on the structural behaviour of concrete dams is a problem of growing interest, which is greatly stimulated by dam ageing. Indeed, the presence of cracks in a dam can be a source of uncertainty regarding its durability, functional operation, and structural stability. A dam with a state of significant cracking and showing signs of distress may in a particular case such as an earthquake or a flood creates a major disaster. To decide whether the structure needs rehabilitation, one must compute efficiently if the cracks present a real issue for the stability of the structure. The method used to model crack initiation and propagation must be robust and must take into account the particularities that cracks have in hydraulic structures such as pressurized water penetration.

This paper presents a crack model that couples the benefits of the damage mechanic approach and the extended finite element method

(XFEM) [1]. Beside the use of the regularized XFEM model [2], XFEM models presented to date used most often a linear elastic fracture mechanics (LEFM) approach to enrich the crack tip. Although large concrete structures like dams are often cited as possible candidates for application of LEFM models, there are severe limitations to this approach because of the extent of the fracture process zone (FPZ) in relation to the size of the structure. Herein, the proposed constitutive models makes use of the non linear fracture mechanics (NLFM) approach in the FPZ by using a classical damage mechanics approach and makes the transition to XFEM when the concrete has reached a certain level of damage. The transition from NLFM to XFEM may also be interpreted as the time when coalescence of micro-cracks occurs to give a true discrete crack. Hence, the use of the damage mechanics approach in the FPZ does not require special crack tip enrichment based on stress intensity factors and fracture toughness material properties difficult to define. Damage mechanics gives a predictor for the crack path and helps compute level set functions. The XFEM formulation with simple Heaviside function enrichment in the completely open region avoids the shear locking phenomenon often observed with smeared type models. Moreover, it does not require remeshing and the mechanical crack mouth opening displacement (CMOD) can be computed accurately for hydro-mechanical coupling.

2 Continuum damage model

The benefit of a continuum damage approach is the possibility to model areas where the damage causes a multitude of micro-cracks that are not necessarily localized. A good example of this phenomenen is the damage caused by thermal gradients on the surface of a structure. The damage is present, but often no dominant crack grows. This kind of behaviour would be very complex to model with the XFEM. If damage is localized, then prevailing crack grows and the XFEM can adequately model the crack. Another benefit of the continuum damage model is its ability to efficiently predict and adjust initial predictions of crack directions during their evolutions.

The rotating anisotropic damage model considered in this paper is similar to that presented by Gunn [3]. The effective stress $\bar{\boldsymbol{\sigma}}$ for an isotropic damage model is defined as:

$$\bar{\boldsymbol{\sigma}} = (1-d)\,\boldsymbol{\sigma} \tag{1}$$

where $\boldsymbol{\sigma}$ is the total stress and d is the scalar damage index that is equal to zero when the material is undamaged and to one when it is completely damaged. In the case of an anisotropic formulation, the damage index is given by a tensor and can be written in the following form:

$$\bar{\boldsymbol{\sigma}} = \boldsymbol{M^{-1}} : \boldsymbol{\sigma} \tag{2}$$

with $\mathbf{M}$ the damage tensor. The total stress $\boldsymbol{\sigma}$ is computed in terms of the elastic stress-strain relationship:

$$\boldsymbol{\sigma} = \boldsymbol{C_0} : \boldsymbol{\epsilon} \tag{3}$$

with $\mathbf{C}_0$ the usual linear-elastic constitutive tensor. In the case of a damaged material, the stress-strain relationship is given by:

$$\boldsymbol{\sigma} = \boldsymbol{C_d} : \boldsymbol{\epsilon} \tag{4}$$

where $\mathbf{C}_d$ is the damaged constitutive tensor. Using the previous relations, the damaged consitutive tensor can be evaluated as follows:

$$\boldsymbol{C_d} = \boldsymbol{M^{-1}C_0} \tag{5}$$

To keep the damaged constitutive tensor symetric, one can, with the principle of energy equivalence [4], replace it by a symetric tensor given by:

$$\boldsymbol{C_d} = \boldsymbol{M^{-1}C_0}\left(\boldsymbol{M^{-1}}\right)^{\boldsymbol{T}} \tag{6}$$

Damage is initiated when a tensor norm is greater than the initial threshold r_0. The tensor norm must take into consideration the behaviour of concrete in tension and compression. Thus, one suitable norm that takes into consideration the effect of compressive strains and defined as the equivalent strain $\bar{\tau}$, as proposed by Ghrib [5], can be written as follows:

$$\bar{\tau} = \sqrt{\sum_{i=1}^{2}\left(\langle\varepsilon_i\rangle^2 + m\langle-\varepsilon_i\rangle^2\right)} \tag{7}$$

where ε_i are the principal strains, with $\langle \dots \rangle$ the Macaulay brackets: $\langle \varepsilon_i \rangle = \varepsilon_i$ if $\varepsilon_i > 0$, $\langle \varepsilon_i \rangle = 0$ if $\varepsilon_i < 0$ and m is introduced to consider that the effect of compressive strains are smaller than tensile strains and is defined by:

$$m = \left(\frac{f'_t}{f'_c} \right)^2 \tag{8}$$

with f'_t, the tensile strength and f'_c the compressive strength. The damage evolution function is given by:

$$d = 1 - \sqrt{\frac{r_0}{\bar{\tau}} \exp\left(-C\left(\bar{\tau} - r_0\right)\right)} \tag{9}$$

The initial threshold is defined in terms of the tensile strength and the elastic modulus:

$$r_0 = \frac{f'_t}{E_0} \tag{10}$$

with E_0, the elastic modulus and C is given by the relation:

$$C = \frac{2}{r_0 \left(\dfrac{2 G_f E_0}{l_{\text{rve}} f_t^2} - 1 \right)} \geq 0 \tag{11}$$

where G_f is the fracture energy and corresponds to the area under the stress-strain curve, l_{rve} the representative volume element characteristic length. The damage evolution is based on the principal strains exceeding the damage threshold r_0 :

$$\begin{aligned} &\bullet \text{ if } \varepsilon_1 > r_0 \text{ then } d_1 = d \\ &\bullet \text{ if } \varepsilon_2 > r_0 \text{ then } d_2 = d \end{aligned} \tag{12}$$

Now the anisotropic damage tensor can be defined by:

$$\mathbf{M} = \begin{bmatrix} \frac{1}{1-d_1} & 0 & 0 \\ 0 & \frac{1}{1-d_2} & 0 \\ 0 & 0 & \beta \end{bmatrix} \tag{13}$$

with $\beta = \sqrt{\frac{1}{2}\left(\frac{1}{(1-d_1)^2} + \frac{1}{(1-d_2)^2} \right)}$. Damage in either of the principal directions leads to a reduction of shear resistance by the coefficient β similar to that found in smeared crack models. The damage tensor is valid in the local reference frame (aligned with the principal strains directions). Hence, in the global reference frame, this tensor must be rotated by the transformation matrix given by:

$$\mathbf{T} = \begin{bmatrix} l_1^2 & m_1^2 & l_1 m_1 \\ l_2^2 & m_2^2 & l_2 m_2 \\ 2 l_1 l_2 & 2 m_1 m_2 & l_1 m_2 + l_2 m_1 \end{bmatrix} \tag{14}$$

with the direction cosine $\varepsilon_1 = \{l_1, m_1\}$, $\varepsilon_2 = \{l_2, m_2\}$. The transformation from the local to the global reference frame of the damaged constitutive tensor is given by:

$$\mathbf{C}_d^{(g)} = \mathbf{T}^{\mathrm{T}} \mathbf{C}_d^{(l)} \mathbf{T}_l \tag{15}$$

Finally, it is considered that the damage is distributed on a representative volume element l_{rve}. Therefore this measure is given by the relation:

$$l_{\text{rve}} = \sqrt[2]{V_e} = \sqrt[2]{\sum_{i=1}^{n_{int}} w_i \det{}_i} \tag{16}$$

with V_e the element volume, n_{int} the number of integration points, w the weight and $\det$ the determinant associated with the Gauss point. Similarly, the equivalent strain $\bar{\tau}$ is averaged over the volume and is given by:

$$\bar{\tau}^{av} = \frac{\sum_{i=1}^{n_{int}} \bar{\tau}_i w_i \det{}_i}{\sum_{i=1}^{n_{int}} w_i \det{}_i} \tag{17}$$

3 XFEM representation of the discontinuity

In contrast with the continuum damage model where the damage is distributed over a representative element volume, the XFEM allows to represent a discontinuous displacement field across a localized crack. Thus, when the coalescence of micro-cracks occurs a true open discrete crack can be well represented with the XFEM. The basis of this method is related to the concept of partition of unity [6] to enrich the finite element method. A partition of unity

in a domain Ω is a set of functions $\varphi_I(x)$ such that:

$$\sum_{\forall I} \varphi_I(x) = 1, \ \forall x \in \Omega \tag{18}$$

The property of a partition of unity is that any function $\psi(x)$ can be reproduced by a product of the partition of unity function with $\psi(x)$. So the standard finite element approximation can be enhanced by introducing additional unknown a_I to the problem:

$$u^h(x) = \underbrace{\sum_{\forall I} N_I(x) u_I}_{u^{EF}} + \underbrace{\sum_{\forall I} \varphi_I(x)\psi(x) a_I}_{u^{enr}} \tag{19}$$

with N_i the standard shape functions of the finite element method and u_I the standard degrees of freedom of the problem. The first part of the right hand side of equation (19) represents the approximation of the standard finite element method, while the second part is the enrichment. The nodal values a_I are the additional degrees of freedom that adjust the enrichment so that they approximate the function $\psi(x)$. In the partition of unity finite element method (PUFEM) [6] the enhancement is global while in contrast the XFEM [1] uses a local partition of unity, that is enrichment is added only if required.

To represent a strong discontinuity such as a crack, the Heaviside function can be used for $\psi(x)$:

$$H(z) = \begin{cases} 1, & z > 0 \\ 0, & \text{else} \end{cases} \tag{20}$$

The displacement approximation is given by:

$$\begin{aligned} u^h(x) = &\sum_{\forall I} N_I(x) u_I + \sum_{J \in S_H} N_J(x) \\ &\left[H(f(x)) - H(f(x_J))\right] a_J \end{aligned} \tag{21}$$

where S_H represents the set of nodes that are enriched because the discontinuity passes through the element they are attached to and x_J is the position of node J

For elements cut by the crack, the jump in the displacement field across the crack Γ_d is thus given by the equation:

$$\left[|u^h(x)|\right]_{\Gamma_d} = \sum_{J \in S_H} N_J(x) a_j, \ x \in \Gamma_d \tag{22}$$

In equation (21) the enrichment function is shifted so that the product of the shape function N_I and the enrichment function cancels out at each node, as proposed in the reference [7] Therefore, only those elements that are crossed by the discontinuity should be treated differently.

Another enrichment can be used for the crack tip but as these functions are based on LEFM, they will be omitted in this paper. Instead, the crack tip will always be located on the edge of an element and the stress field beyond the tip will be computed with the continuum damage model (micro-cracks in the FPZ).

4 Crack tracking technique

The prediction of the crack direction for crack propagation is an important key to have a successful model. To avoid the lack of crack localisation, the solution algorithm must promote it to develop along a minimal number of finite element rows. Thus the crack tracking technique must indicate the finite elements that can potentially be crossed by a crack. The position of the crack within the element can be evaluated with level-sets [8]. This ensures the continuity of the crack between the elements and once the level of damage has reached a certain threshold, these level-sets can directly be used for the XFEM formulation.

4.1 Location of a new potential crack root

We first make the assumption that cracks initiate along boundaries. Thus a potential crack root can be identified on the boundary mesh by a tensile energy criterion similar to that of reference [9]:

$$\frac{1}{2}\sigma_1 \epsilon_1 \geq \gamma U_0 \tag{23}$$

where γ is a threshold factor to identify potential elements. If γ is close to one, then more Newton iterations will be required for convergence in a load step because the crack will advance element by element. In the other hand, if

γ is set too low, many elements will be identified and there is a chance that the crack diffusion will be high. Numerical experiments has shown that $\gamma = 0.85$ works well. When multiple elements on the boundary exceed the criterion, the one that has the greatest tensile energy is selected as the crack root for that iteration. Once a root element is selected, the coordinates of the crack origin $o(x, y)$ must be computed. We make the assumption that the origin is located at the center of the element edge located on the boundary. If more than one edge is in contact with the boundaries, the centroid of the element is selected as the origin. Knowing the origin point and the crack normal $\vec{n}$, the level-set ϕ can be defined. In this paper the principal equivalent stress (similar to the equivalent strain given by the relation (17) direction cosine is taken as the crack normal direction. Thus a plane passing through point $o(x, y)$ and with a normal $\vec{n}$ is defined by the equation:

$$d = -\vec{n} \cdot o(x, y) \tag{24}$$

The level-set, defined by the signed distance (point-plane distance) can be evaluated for all the potential root element nodes. For example, at node i with coordinates $p(x, y)$ the signed distance is given by the relation:

$$\phi_i = \frac{\vec{n} \cdot p(x, y) + d}{||\vec{n}||} \tag{25}$$

4.2 Potential crack propagation

Now that the root element is found, its level set at every nodes computed, the identification of the potential crack path can be defined. The neighbour element whose edge respect the condition $\min(\phi_i) \times \max(\phi_j) < 0$ is selected (its minimal level-set times its maximal one is less than zero). If this neighbour element energy threshold (23) is exceeded, than the element nodes level-sets not already computed can be evaluated similarly to that previously defined. Particular attention must be taken to scale the level-sets at these nodes. The signed distance is evaluated by the point-plane distance. Hence, the element nodes do not necessarily lie at the same signed distance of two different planes. Consequently, the ratio of the level-set at a node already defined with the level-set it would have if it would be computed with the new plane is the scaling factor to apply on the newly defined level-set for this element. The potential crack propagation can be cycled until all the element in the neighbourhood of the crack tip do not respect the threshold defined in equation (23).

4.3 Maximum curvature criterion

Similar to that in reference [10], a maximum curvature criterion is introduced to correct spurious changes in propagation direction. If the current considered element crack normal $\vec{n}_e$ makes an angle larger than α_{max} with the normal of the previous element $\vec{n}_p$ considered along the crack path, then the modified normal $\vec{n}_m$ of the current element is defined as:

$$\begin{bmatrix} (n_m)_x \\ (n_m)_y \end{bmatrix} = \begin{bmatrix} \cos(\alpha) & -\sin(\alpha) \\ \sin(\alpha) & \cos(\alpha) \end{bmatrix} \begin{bmatrix} (n_p)_x \\ (n_p)_y \end{bmatrix} \tag{26}$$

where the rotation angle is defined by $\alpha = \text{sign}((\vec{n}_p \otimes \vec{n}_e)_z)\frac{\alpha_{max}}{2}$. The direction of the rotation is simply given by the sign of the z component of the vector given by the cross product of the previous element normal with that of the current element normal.

4.4 Predictor corrector

The element can sustain damage as presented in section 2 if it respects the condition $\min(\phi_i) \times \max(\phi_j) < 0$. The initial equivalent principal stress direction used to computed the level-sets is susceptible to change in a rotating crack model. Given this change of direction, the crack root found in the previous section is the starting point for the crack propagation until a certain level of damage threshold $d > \eta$ is attained. Hence, when this threshold is obtained, the level-sets are fixed for the element. As the level-sets need not be updated, the root element can be defined as the next element in the crack path where this threshold is not exceeded. Therefore, the potential crack path is predicted in section 4.2 and is corrected according to the damage sustained by the elements

crossed by the crack by cycling the propagation algorithm again at each Newton iteration.

5 Transition from continuum damage mechanics to XFEM

In this paper the transition from continuum damage mechanics to XFEM formulation does not have any special treatment. Hence, the total energy dissipation in the process is approximately correct. If this transition occurs at a time where the damage is high ($d \simeq 1.0$), the energy dissipation for the element is almost completed. Hence, the error introduced in energy balance is of small amplitude. This issue will be investigated in the numerical results presented in the next section.

6 Validation examples

Three validation examples are presented in this section. The simple three point beam tested by Bažant and Pfeiffer [11], the shear beam with single notch tested by Arrea and Ingraffea [12] and the tension-shear specimen tested by Nooru-Mohamed [13] are used for the validation of the proposed model. For all the validation examples, the parameters are fixed. Thus, α_{max} is fixed to 20°, the level-sets are fixed for the element when the scalar damage index has reached $d > \eta > 0.60$ and finally the transition from continuum damage mechanics to XFEM formulation occurs when the scalar damage index reaches $d > 0.95$.

6.1 Three point beam

The beam in figure 1 tested by Bažant and Pfeiffer [11] with d =0.3048 m and a thickness of 0.038 m is considered for the first validation example. The material properties are given in table 1.

Table 1: Material properties for the three-point beam specimen

E (MPa)	f_t' (MPa)	f_c' (MPa)	ν	G_f (N/m)
27413	2.886	34.0	0.18	40.29

Displacement control has been performed by applying a displacement increment $\Delta u = 4 \times 10^{-6}$ at the two nodes adjacent to the center line of the beam. In the experiment, the ultimate average load resistance was $P_u = 7784$N. Four different Q4 plane stress meshes were used to study the results independence with regards with the mesh refinement. The computed ultimate loads are 6516 kN, 6538 kN, 7093 kN and 7625 kN, respectively for $h_c = d/6$, $d/12$, $d/24$ and $d/36$. The ultimate loads computed are in the range of the experimental one and given that the finest mesh is six times more refined than the coarsest one, the results are nearly mesh independent.

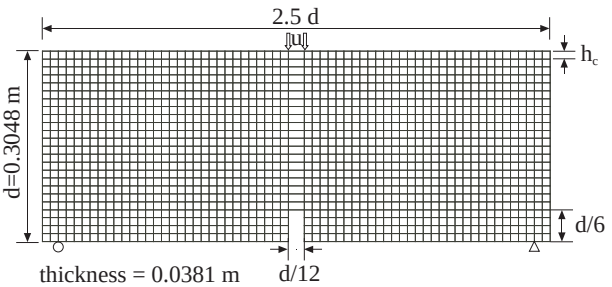

Figure 1: Notched three-point beam specimen dimensions (mesh $h_c = d/24$)

The force-displacement curve for the case where $h_c = d/36$ is given in figure 2. Continuum damage model results are compared with the XFEM+damage model. The responses are almost identical until the transition occurs in the first element (at 0.12 mm). The slope of the softening is greater with the model that uses XFEM. This is a direct consequence of the transition that does not take account of energy transfer. In this case, the results are marginally affected.

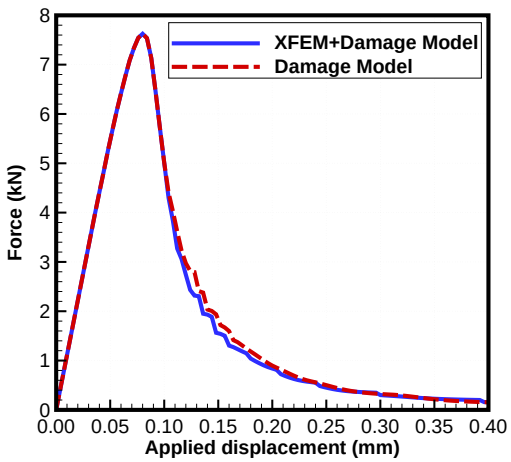

Figure 2: Force-displacement response of the beam

6.2 Shear beam with single notch

A single-notched shear beam illustrated on figure 3 tested by Arrea and Ingraffea [12] which failed in curved mode I fracture is used as a second validation example. Most smeared crack solutions are unable to predict full separation and softening down to zero [14]. Hence, the transition from damage mechanics to XFEM should be able to alleviate this problem. The crack mouth sliding displacement (CMSD) is used as a feed-back signal to control the load applied and capture the snap-back response of the beam. The material properties are given in table 2.

Table 2: Material properties for the shear beam specimen

E (MPa)	f_t' (MPa)	f_c' (MPa)	ν	G_f (N/m)
24800	2.80	45.5	0.18	100

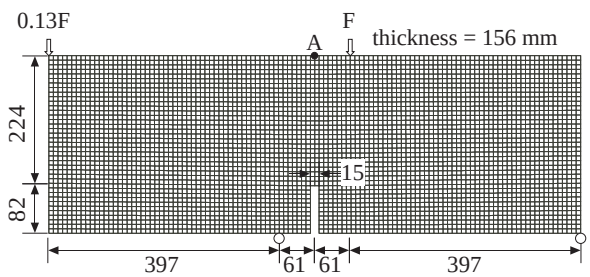

Figure 3: Shear beam with single notch specimen dimensions

The beam model meshed with Q4 plane stress elements is used to compute the force-CMSD response of the shear beam with three constitutive model. The first model uses continuum damage mechanics with no special crack tracking technique. The second model uses the crack technique presented previously with a continuum damage mechanics model. The last model, is similar to the second one but makes transition from damage mechanics to XFEM when the threshold level of damage is reached. The force-deflection of point A response curves are presented in figure 4 for the three models and compared with the discrete crack model results given in reference [14]. The model with no special treatment of the crack path is unable to predict the beam snap-back. The ultimate load predicted with this model (80 kN) is low compared to the experimental results (average of 130 kN). The two models that makes use of the special treatment of the crack path predict the same ultimate load (118 kN) but the continuum damage model is unable to predict the snap-back and load-displacement response to zero fails. The third model gives results that are in agreement with those presented by Rots [14]. Thus, the softening down to zero in this case is only possible with the XFEM formulation.

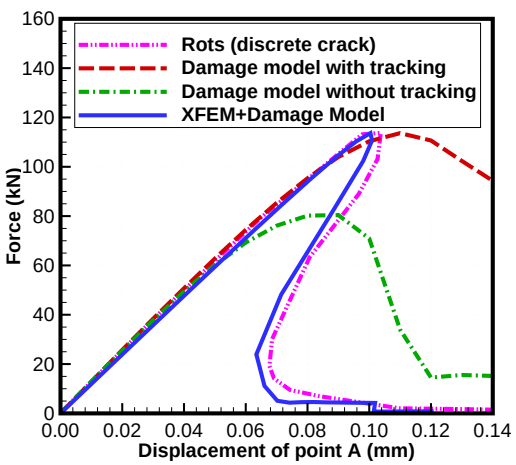

Figure 4: Force-deflection of point A of the shear beam

The crack path computed without the crack tracking technique is given in figure 5. The path is compared with the profile observed in

the laboratory and used by Rots for the discrete crack analysis performed by introducing interface elements on the *a priori* known crack path. The profile computed is not in agreement with the experimental one. It starts to propagate vertically and turns slowly in the direction of the applied load. This explains the discrepancy of the ultimate load predicted with this model. Figure 6 gives the profile computed with the special crack tracking technique and the XFEM+damage model. The crack path is almost identical with the experimental one. Hence, a special crack tracking technique is required to compute an accurate crack profile for this validation case.

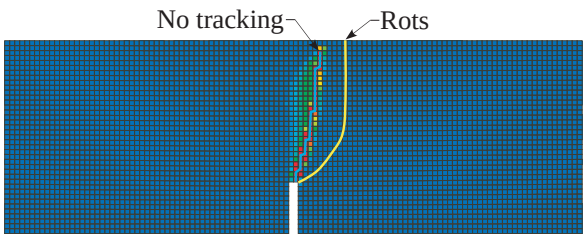

Figure 5: Crack path predicted without special crack tracking technique (Damage)

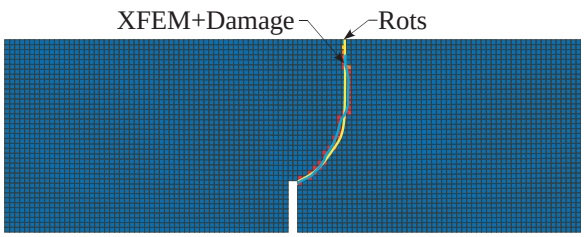

Figure 6: Crack path predicted with special crack tracking technique (XFEM+damage)

6.3 Crack propagation in a tension-shear specimen

A tension-shear specimen made of concrete tested experimentally by Nooru-Mohamed [13] is taken as the last validation example to demonstrate the applicability of the model. The geometry, the loading and boundary conditions of the panel are presented in figure 7. The material parameters, similar to those used in reference [15], are given in table 3. Loading is applied via prescribed displacements along the left edge and the top edge of the panel. The prescribed u_x displacement on the left edge is applied in a manner to have the shear force $P_{,s}$ constant at all time and the displacement on the top edge is varied continuously. The model is meshed with Q4 plane stress elements.

Table 3: Material properties for the tension-shear specimen

E (MPa)	f'_t (MPa)	f'_c (MPa)	ν	G_f (N/m)
30000	3.00	30.0	0.20	110

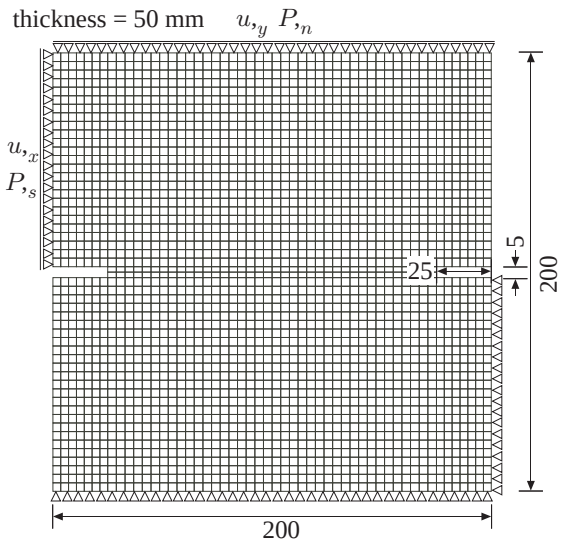

Figure 7: Tension-shear specimen dimensions

Load displacement responses for loading paths 4a to 4c are presented in figures 8 to 10 and are compared with the experimental results and those of reference [16]. The ultimate load for loading path 4a is slightly over estimated, while that of loading path 4b is in agreement with the experimental one. For loading path 4c, the experimental specimen failed in pure shear mode. Hence, the experimental ultimate resistance in tension is 0. A small tension force in combination with the shear force is required in the numerical model to initiate the crack. Hence, a traction of 2 kN is applied. For the softening part of the curves from all loading paths, it is obvious that more energy is dissipated in the transition process from damage mechanics to XFEM when the cracks progress and the force-displacement curves fall below the experimental one.

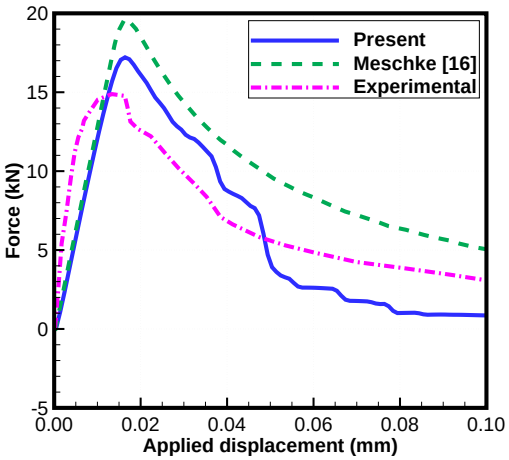

Figure 8: Load-displacement for loading path 4a ($P_{,s}$=5kN)

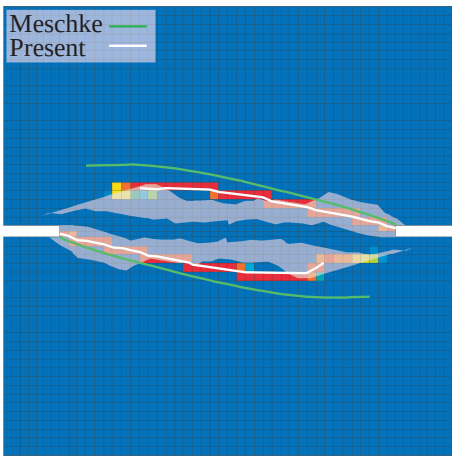

Figure 11: Computed crack path for loading path 4a ($P_{,s}$=5kN)

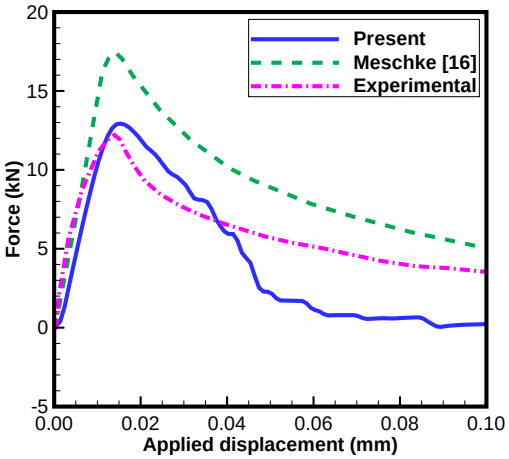

Figure 9: Load-displacement for loading path 4b ($P_{,s}$=10kN)

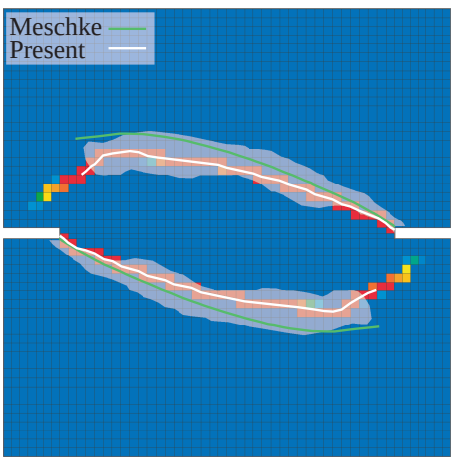

Figure 12: Computed crack path for loading path 4b ($P_{,s}$=10kN)

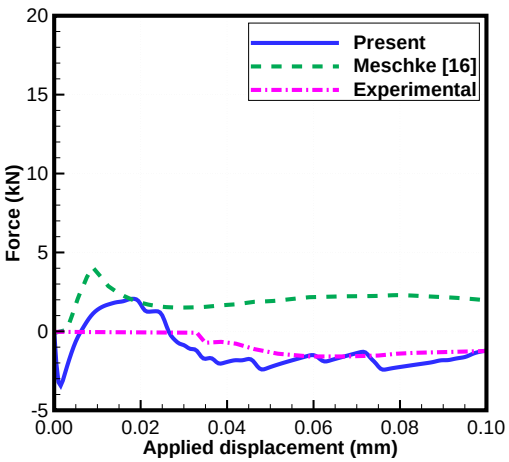

Figure 10: Load-displacement for loading path 4c ($P_{,s}$=27.5kN)

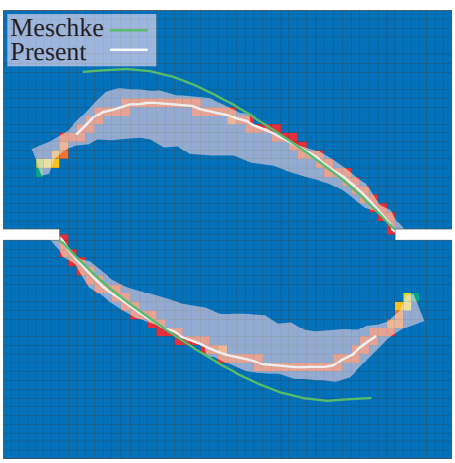

Figure 13: Computed crack path for loading path 4c ($P_{,s}$=27.5kN)

Figures 11 to 13 contains the crack trajectories from all three tests obtained from the analyses. The experimentally observed crack paths are included in shaded color. The computed trajectories are in agreement with the experimental ones for all loading paths.

7 Conclusion

The proposed model has shown the following features:

- The localized cracks predicted by the proposed tracking technique are consistent with the ones experienced in structures. The cracks develop along a single row of finite elements and minimum diffusion of damage is observed;
- The transition to XFEM when the damage is important alleviate the locking phenomenon often observed in smeared type models;
- The model has the ability to predict the crack path with a damage mechanics model and because the rotating crack model is used, the crack direction can be corrected;
- The validation examples have shown the efficiency and the robustness of the model.

However, more work must be done for the transition from continuum damage mechanics to XFEM formulation to conserve the total energy dissipation in the fracture process. It was shown that energy dissipation can have influence on the softening behaviour of the constitutive model.

REFERENCES

[1] T. Belytschko and T. Black, 1999. Elastic crack growth in finite elements with minimal remeshing. *International Journal for Numerical Methods in Engineering, Int. J. Numer. Meth. Engng.*, 45(5):601–620.

[2] Borek Patzák and Milan Jirásek, 2003. Process zone resolution by extended finite elements. *Engineering Fracture Mechanics*, 70(7-8):957–977.

[3] R. M. Gunn, 1998. *Non-linear analysis of arch dams including an anisotropic damage mechanics based constitutive model for concrete*. PhD thesis, University of Brighton, U.K.

[4] Sidoroff F. Cordebois C., 1979. Endommagement anisotrope en élasticité et plasticité. *Journal de Mécanique appliquée*, 25:45–60.

[5] Faouzi Ghrib, 1994. *Sur l'analyse de la fissuration des barrages en béton par la mécanique de l'endommagement continu-comportement statique et dynamique*. PhD thesis, Dept. de génie civil, École Polytechnique de Montréal, Montréal, Québec, Canada.

[6] I. Babuška and J. M. Melenk, 1997. The partition of unity method. *International Journal for Numerical Methods in Engineering*, 40(4):727–758.

[7] Ted Belytschko, N. Moës, S. Usui, and C. Parimi, 2001. Arbitrary discontinuities in finite elements. *International Journal for Numerical Methods in Engineering, Int. J. Numer. Meth. Engng.*, 50(4):993–1013.

[8] Stanley Osher and James A Sethian, 1988. Fronts propagating with curvature-dependent speed: Algorithms based on Hamilton-Jacobi formulations. *Journal of Computational Physics*, 79(1):12–49.

[9] Sudip S. Bhattacharjee and Pierre Leger, apr 1994. Application of NLFM Models to Predict Cracking in Concrete Gravity Dams. *Journal of Structural Engineering, J. Struct. Eng.*, 120(4):1255–1271.

[10] Roberto Clemente Miguel Cervera, Luca Pelà and Pere Roca, 2010. A crack-tracking technique for localized damage

in quasi-brittle materials. *Engineering Fracture Mechanics*, 77(13):2431 – 2450.

[11] Zdenek P. Bazant and Phillip A. Pfeiffer, 1987. Determination of Fracture Energy from Size Effect and Brittleness Number. *ACI Materials Journal*, 84(6):463–480.

[12] M. Arrea and A.R. Ingraffea, 1981. Mixed-mode crack propagation in mortar and concrete. Technical Report Report 81-13, Department of Structural Engineering, Cornell University, Ithaca, New York.

[13] M. B. Nooru-Mohamed, 1992. *Mixed-mode fracture of concrete: an experimental approach*. PhD thesis, Delft University of Technology, Delft, The Netherlands.

[14] J. G. Rots, 1988. *Computational Modeling of Concrete Fracture*. PhD thesis, Delft University of Technology, Delft, The Netherlands.

[15] G. Hofstetter C. Feist, 2003. Mesh-insensitive strong discontinuity approach for fracture simulations of concrete. International Conference on Numerical Methods in Continuum Mechanics (NMCM 2003). V. Kompis, J. Sladek, M. Zmindak Ed.

[16] Günther Meschke and Peter Dumstorff, 2007. Energy-based modeling of cohesive and cohesionless cracks via X-FEM. *Computer Methods in Applied Mechanics and Engineering*, 196(21-24):2338 – 2357.